European Radiology (2019) 29:3224–3232
https://doi.org/10.1007/s00330-018-5885-1

MUSCULOSKELETAL

Muscle diffusion tensor imaging in glycogen storage disease V (McArdle disease)

R. Rehmann[1] · L. Schlaffke[1,2] · M. Froeling[2] · R. A. Kley[1] · E. Kühnle[1] · M. De Marées[3] · J. Forsting[1] · M. Rohm[1] · M. Tegenthoff[1] · T. Schmidt-Wilcke[4,5] · M. Vorgerd[1]

Received: 30 August 2018 / Revised: 18 October 2018 / Accepted: 13 November 2018 / Published online: 17 December 2018

Abstract

Purpose To evaluate differences in diffusion parameters in thigh muscles in patients with glycogen storage disease type V (McArdle disease) using muscle diffusion tensor imaging (mDTI) compared to healthy controls

Methods In this prospective study, we evaluated thigh muscles from hip to knee of 10 McArdle patients (5 female, mean age 33.7 ± 14.4 years) and 10 healthy age- and gender-matched volunteers. MRI scans were performed at 3 T and comprised mDTI, T1-weighted and T2-weighted imaging between May 2015 and May 2017. Needle biopsy of the vastus lateralis muscle was performed in three McArdle patients. The muscle tissue was analyzed by using histochemical and enzyme-histochemical techniques for glycogen content and histopathological changes. Mean values of the eigenvalues (λ_1–λ_3), fractional anisotropy (FA), and mean diffusivity (MD) were obtained for the vastus lateralis, vastus medialis, rectus femoris, biceps femoris, semitendinosus, and semimembranosus and compared between groups using Student's *t* tests, as well as ANCOVA; significance level was set at $p < 0.05$.

Results Needle biopsy showed intracellular glycogen accumulation in skeletal muscle fibers of three McArdle patients. Extracellular histopathological changes were not found. Muscle DTI analysis did not show statistically significant differences between patients and controls for any of the muscles.

Conclusion Despite intracellular glycogen accumulation in the three biopsy samples, mDTI parameters were not altered in McArdle patients compared to controls. We conclude that the currently used mDTI acquisition and processing lack the sensitivity to detect intracellular changes due to accumulated glycogen in this cohort of McArdle patients.

Key Points

- *Despite intracellular glycogen accumulation in three examined biopsy samples, mDTI parameters were not altered in McArdle patients compared to controls.*
- *In its current form, diffusion MR does not provide additional information in quantifying intracellular glycogen accumulations within skeletal muscle fibers in McArdle patients.*

Keywords Muscle · Diffusion tensor imaging · Anisotropy · Glycogen storage disease

R. Rehmann and L. Schlaffke contributed equally to execution of the project.

T. Schmidt-Wilcke and M. Vorgerd contributed equally to study conceptualization.

Electronic supplementary material The online version of this article (https://doi.org/10.1007/s00330-018-5885-1) contains supplementary material, which is available to authorized users.

✉ L. Schlaffke
lara.schlaffke@ruhr-uni-bochum.de

[1] Department of Neurology, BG-University Hospital Bergmannsheil, Ruhr-University Bochum, Bochum, Germany

[2] Department of Radiology, University Medical Centre Utrecht, Utrecht, The Netherlands

[3] Department of Sports Medicine and Sports Nutrition, Faculty of Sport Science, Ruhr-University Bochum, Bochum, Germany

[4] St. Mauritius Therapieklinik, Meerbusch, Germany

[5] Institute of Clinical Neuroscience and Medical Psychology, Heinrich Heine University of Düsseldorf, Düsseldorf, Germany

Abbreviations

ATP	Adenosine triphosphate
CK	Creatine kinase
FA	Fractional anisotropy
GSD	Glycogen storage disease
HE	Hematoxylin and eosin
MD	Mean diffusivity
mDTI	Muscle diffusion tensor imaging
PAS	Periodic acid-Schiff
PFK	Phosphofructokinase
PL	Phosphorylase
TC	Trichrome Gomori

Introduction

McArdle disease is a rare hereditary glycogen storage disease (GSD V) with an estimated prevalence of 1:100,000–350,000 (USA and the Netherlands).

Next-generation sequencing data even suggest a higher incidence (1:50,000), and thus, it could be an underdiagnosed condition [1]. McArdle disease affects the glycogen metabolism in skeletal muscle due to mutations in the glycogen phosphorylase gene [2–4]. Glycogen phosphorylase catalyzes the first step of intramuscular glycogen breakdown. Thus, a deficiency leads to myocellular glycogen accumulation and causes a lack of energy generated from intramuscular glycogen [5, 6].

Clinical symptoms are exercise intolerance, muscle pain, and cramps. The failure of ATP production during muscle exercise can subsequently cause rhabdomyolysis [6].

Symptom severity varies, and approximately 85% of the patients experience symptoms before the age of 10 years, but around 50% of those patients were first diagnosed after the age of 30 years [2].

Diagnosis is based on clinical symptoms, elevated serum creatine kinase (CK) levels, and missing lactate increase in anaerobic exercise and confirmed by genetic testing and/or muscle biopsy [7]. So far, there is no treatment option to cure the disease. Standard therapy includes physiotherapy and aerobic muscle exercise [8]. Various dietary concepts such as carbohydrate-rich diet and supplementation of sucrose and ribose showed no clear effect [9]. However, a ketogenic diet and creatine supplementation showed an increase in muscle activity tolerance in case reports and need further investigation [10]. Standard muscle MRI evaluation usually shows no muscle edema or fatty infiltration. During a long-term disease course, there can be fatty replacement of lower leg and shoulder girdle muscles [11, 12].

Thus, standard clinical MRI does not allow for disease differentiation or therapy monitoring. Up to now, only C^{13} and P^{31} magnetic resonance spectroscopy could show altered glycogen accumulation and metabolism in McArdle disease in a non-invasive manner [13–17]. However, multinuclei spectroscopy requires additional hardware and is not broadly available. To contribute to an early disease evaluation, new (quantitative) MR-imaging protocols need to be evaluated.

By quantifying the diffusion properties of water molecules in muscle tissue, muscle diffusion tensor imaging (mDTI) can provide information about muscular microstructure. As such, mDTI is increasingly used in myopathy research [18–20]. It potentially allows for an assessment of disease progression and disease-specific patterns of altered muscle architecture, as well as an early identification of subclinical changes [19, 21–23]. Currently, there is no knowledge about the correlation of diffusion parameters with myocellular architecture in McArdle disease. We hypothesized that the intracellular deposits of glycogen lead to changes in diffusion characteristics of water molecules in muscle fibers.

We therefore aimed to evaluate disease-specific alterations in the mDTI metrics in McArdle disease. We compared mDTI parameters of patients with those of age- and gender-matched healthy controls and obtained muscle needle biopsy data of three McArdle patients to quantify the accumulated glycogen.

Materials and methods

Compliance with ethical standards

This prospective study had been approved by the local ethics committee of Ruhr-University Bochum (No. 15-5281 and for needle biopsy: No. 15-5748), and written informed consent was obtained from all participants prior to enrollment.

Participant data

Ten patients with McArdle disease (5 females, 5 males; mean age 33.7 ± 14.4 years, range 22–45 years) and ten age- and gender-matched healthy controls participated in this study between May 2015 and November 2016 (see Table 1). The patients were recruited in our outpatient clinic for neuromuscular diseases. Inclusion criteria were a histology and/or genetically proven GSD V disease. We excluded patients with diabetes or other additional diseases like myopathies. An experienced neurologist examined each participant; every extremity was tested for grade of strength based on the muscle strength grading scale (Medical Research Council scale, ranging from 5/5, full strength, to 0/5, no visible muscle contraction). The subjects reported no unaccustomed strenuous exercise (like unaccustomed weight lifting or sprinting exercise) 2 days prior to MRI examination.

Needle biopsy

Three McArdle patients agreed to a needle biopsy to evaluate the actual amount of accumulated glycogen within muscle cells and other histopathological changes. Muscle biopsy of the left vastus

Table 1 Demographic data of study participants

	Sex	Age	BMI patient	BMI control	Patient age at first symptoms	Patient age when first diagnosed	Patient experienced rhabdomyolysis	Patient genetic PYGM variation
Pair 1	m	34	24.6	23.9	11	29	N	p.R50X / p.R50X
Pair 2	m	33	27.5	29.4	11	16	Y	p.R50X / p.R50X
Pair 3	f	37	22.5	24.2	12	31	Y	N/A
Pair 4	f	30	23.9	21	10	29	Y	p.R50X / p.Lys609X
Pair 5	m	31	29.4	24.3	< 5	25	N	c.1362_1394del / c.1362_1394del
Pair 6	f	45	18.3	24.2	6	43	Y	N/A
Pair 7	f	22	31.5	21.4	6	20	N	p.R650X / p.R650X
Pair 8	m	22	23.8	22.1	19	19	Y	p.Ile513Val / p.Ala670Val
Pair 9	f	43	23	20.2	14	17	Y	p.R50X / p.R50X
Pair 10	m	40	26.3	26	< 5	12	N	p.Arg50X / p.Gly686Arg

N no, *Y* yes, *N/A* not available

lateralis muscle between the spina iliaca anterior superior and the cranial margin of the patella was done with a modified Bergström needle akin to Ekblom [24–26]. The biopsy was performed 2 h after the MR acquisition. A T1-weighted (T1w) image served to predefine biopsy localization. The skin was cleaned and shaved. After disinfection, a local anesthesia was performed by injecting 2 cm^3 of xylocaine (2%) and adrenalin (1:100,000). After 20 min of rest, the Bergström needle was placed more than 2 cm below the fascia.

Histochemical and enzyme-histochemical techniques were performed on 10-μm-thick cryosections stained with hematoxylin and eosin (H&E), modified trichrome Gomori (TC), periodic acid-Schiff (PAS) technique, and ATPase reactions preincubated at pH 4.3 and 9.6. The H&E staining allowed detecting myopathic alterations if present. The PAS staining revealed intracellular glycogen accumulation if present. The histochemical analysis of phosphorylase activity (PL) allowed detecting a lack of PL enzyme activity, and the histochemical analysis of phosphofructokinase activity served as an internal control. Stained samples were examined with an Olympus BX61 bright-field microscope (Olympus, Hamburg, Germany). The histological examination was done by a neurologist (MV, 18 years of experience in analyzing muscle and nerve biopsy sections and elected member of the German reference center for neuromuscular diseases of the German Society of Neuropathology and Neuroanatomy (DGNN)).

MRI protocol

MRI was performed using a 3-T MRI (Achieva 3 T X, Philips Medical Systems) and a 16-channel Philips TorsoXL coil. Subjects were placed in a feet-first supine position with the coil covering their thighs, with 8 channels placed posterior and 8 channels placed anterior [21]. To reduce leg movements, a strap was wrapped around the ankles. The participants rested 20–30 min in a sitting position prior to the MR examination.

The full thigh region from hip to knee was split into three non-angulated fields of view (FOV) of 480 × 264 × 150 mm^3 along the *z*-axis (stacks) to avoid shimming artifacts occurring due to a large FOV. The stacks had a 10-mm overlap to allow accurate merging [21, 27]. The MRI acquisition protocol for each FOV comprised T1-weighted (T1w) and T2-weighted (T2w) as well as diffusion-weighted imaging (DWI), with a total acquisition time of approximately 27 min for both thighs (9 min per FOV) with no gaps. T1-weighted (T1w) turbo spin echo (TSE) was acquired first with the following parameters: voxel size 1.5 × 1.5 × 3 mm^3 and TR/TE 1646/15 ms. Next, a T2-weighted TSE sequence with fat suppression (spectral attenuated inversion recovery, SPAIR): voxel size 1.5 × 1.5 × 3 mm^3 and TR/TE 11422/53 ms was acquired. Finally, spin-echo echo planar imaging (SE-EPI) was applied to acquire diffusion-weighted images using the following parameters: voxel size 3 × 3 × 6 mm^3, TR/TE 3819/46 ms, SPAIR fat suppression, SENSE 2, 17 isotropic gradient directions with $b = 400$ s/mm^2, and three non-diffusion-weighted image ($b = 0$ s/mm^2) as well as one noise measurement [28, 29], for SNR calculation (by turning of the RF and imaging gradients).

Data processing

Data was processed using DTITools (*Mathematica 11*) [30]. Data preprocessing was performed akin to that of Schlaffke et al. [27]. In short, the T1w and T2w data of the individual stacks were corrected for motion between the stacks using rigid registration of the overlapping slices. Diffusion data were denoised using a principal component analysis method [31]. Next, the diffusion data was corrected for subject motion and eddy current distortions using affine registration and aligned to T2 data using non-rigid registration (1000 iterations, *b*-spline spacing 120, 80, 80) including the rotation of the *b*-matrix [32]. Finally, the aligned and corrected T1w, T2w, and DWI data were fused by weighted averaging of the overlapping slices, yielding one volume covering the

entire thighs (see Fig. 1). T1w and T2w images were visually inspected for abnormalities and fatty infiltrations.

The diffusion tensor was estimated from the corrected and merged diffusion data using an iterative weighted linear least-square (iWLLS [33]) tensor estimation with outlier detection. From the tensor, the three eigenvectors ν_{1-3} and their scalar, the eigenvalues λ_1–λ_3, were calculated for each voxel. Fractional anisotropy (FA), radial diffusivity (RD), and mean diffusivity (MD) were calculated based on the three eigenvalues. The FA is calculated as $\sqrt{\frac{1}{2}}\frac{\sqrt{(\lambda_1-\lambda_2)^2+(\lambda_2-\lambda_3)^2+(\lambda_3-\lambda_1)^2}}{\sqrt{\lambda_1^2+\lambda_2^2+\lambda_3^2}}$, the RD as $\frac{\lambda_2+\lambda_3}{2}$, and the MD as $\frac{\lambda_1+\lambda_2+\lambda_3}{3}$. The SNR was calculated according to the equation $\frac{mean\ DWI\ signal}{standard\ deviation\ of\ noise\ signal}$ reported by Froeling et al. [34].

Muscle segmentation

In both thighs, six muscles (vastus lateralis, vastus medialis, rectus femoris, biceps femoris, semitendinosus, and semimembranosus) were manually segmented, by drawing regions of interest (ROIs) on every slice of the T1-weighted data set (author MR, 3 years of experience) using 3D Slicer software (3D Slicer 4.4.0, https://www.slicer.org). Muscle segmentation was terminated at the subcutaneous fat and limited to the muscle tissue. The ischiadic nerve, the surrounding connective tissue, and the blood vessels were not included. However, small intramuscular arteries were not further excluded.

The resulting masks were subsequently eroded by one voxel to avoid including fascia tissue. Mean values of the eigenvalues, MD, RD, FA, and the muscle volume were calculated for the entire muscle. Muscle volumes were estimated by the number of voxels in the segmented areas × voxel size.

Statistical analyses

All statistical analyses were performed using IBM SPSS V24. The mDTI parameters FA, MD, λ_1–λ_3, and RD were analyzed in a multivariate general linear model ANCOVA with patient/control as fixed factor and muscle and gender as covariates. Post hoc two-sample Student's *t* tests were performed for each parameter and each muscle between McArdle patients and healthy controls. The significance level was set to $p < 0.05$ for all analyses.

Results

Study participants

All participants were successfully examined; there were no dropouts. Eight of the participating patients had a genetically proven GSD V; two were diagnosed based on histology samples. The average age of the first symptoms was 9 years, whereas the average age of diagnosis was 22.25 years. Six patients reported to have experienced rhabdomyolysis (see Table 1). None of the participants showed fatty infiltrated muscles. BMI, calculated from self-reported height and weight of patients and controls, did not differ significantly ($p = 0.35$). For demographic data of the examined population, see Table 1. All participants (McArdle patients and controls) had a normal physical strength examination of the legs (5/5 on MRC-Muscle Scale for all movements).

Needle biopsy

An example of the needle biopsy histology for one McArdle patient and one healthy volunteer (reference data for the healthy volunteer was from the local muscle bank, not from this study) is shown in Fig. 2. The needle biopsy histochemistry analysis results of all three McArdle patients are reported in Table 2. The patients showed an increased number of fibers with intracellular vacuoles ranging from 4 to 18% of the muscle fibers compared to healthy controls, which stained positive in PAS reactions and thus indicated a glycogen storage disorder.

Enzyme histochemistry revealed an absence of myophosphorylase but normal phosphofructokinase activities, consistent with McArdle disease. In addition, unspecific myopathological findings were present like variability of the diameter of type 1 and type 2 muscle fibers and an increase in

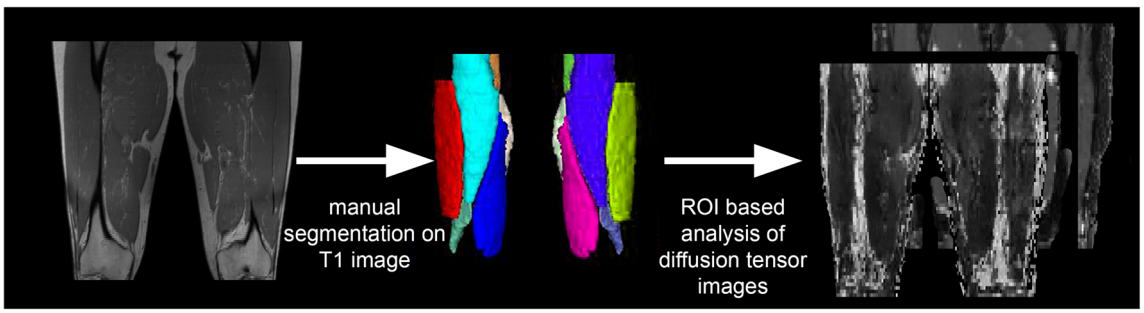

Fig. 1 Post-processing. The muscle masks derived from manual muscle segmentation on a T1w image are registered to the DTI maps to perform ROI-based analysis

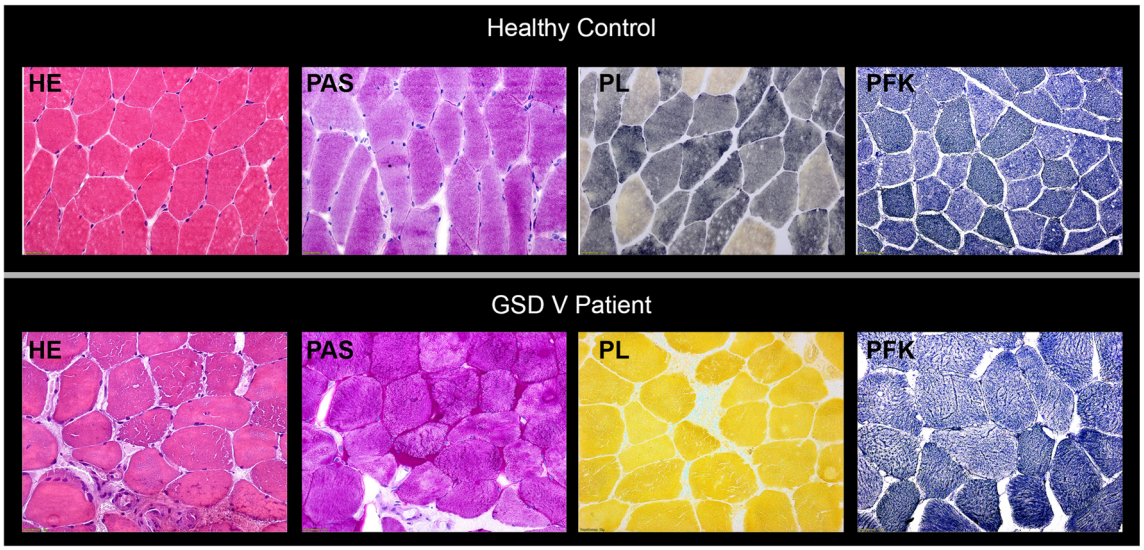

Fig. 2 Histological and enzyme-histochemical staining of muscle needle biopsy (vastus lateralis muscle). Upper row: healthy control (sample out of our local muscle bank); lower row: needle biopsy of a GSD V patient examined in this study (left vastus lateralis muscle). HE, hematoxylin and eosin; PAS, periodic acid-Schiff stain; PL, phosphorylase; PFK, phosphofructokinase stains. HE staining revealed slightly myopathic changes like vacuoles mainly beneath the sarcolemma and some in the center of muscle fibers, some variability of the muscle fiber diameter and a slight increase in the number of centrally located nuclei. PAS staining could show subsarcolemmal glycogen accumulation in the GSD V patient. PL staining revealed a complete absence of phosphorylase, which is typical for GSD V patients. PFK staining showed no difference of the phosphofructokinase enzyme between the healthy control and the GSD V patient

the number of centrally placed myonuclei (see Table 2). Furthermore, type 2 muscle fibers were prone to hypertrophy in up to 57% of the fibers (see Table 2). All three muscle biopsies did not show any extracellular changes, particularly no endomysial or perimysial lipofibromatosis.

mDTI data analysis

Fully automated preprocessing (no user interaction) was successful in all data. Figure 3 (top) shows example raw data of a McArdle patient and the matched healthy control as well as the estimated FA and MD maps.

The mean value of all diffusion values per muscle is shown in Fig. 4 and reported in Table 3 (in Table 3, data for all muscles are pooled; details for each muscle can be found in the supplement). The ANCOVA revealed no significant main effect in any of the assessed parameters between McArdle patients and healthy controls (see Table 4). The average signal-to-noise ratio (SNR) per muscle ranged from 11.3 to 66.7 (mean 39.13 ± 9.2), FA ranged from 0.115 to 0.457 (mean 0.215 ± 0.059), MD ranged from 0.956 to 1.901

Table 2 Needle biopsy data of three GSD V (McArdle) patients

	Muscle fibers with PAS-positive vacuoles (in %)	Muscle fibers with central nuclei (in %)	Extracellular fibrosis?				
Patient 1	6	10	No				
Patient 2	4	14	No				
Patient 3	18	20	No				
	Number of fibers	Diameter (in μm)			Fibers (in %)		
		Min	Max	Mean	Atroph	Normal	Hypertroph
Type 1 fibers							
Patient 1	34	35	81	52	0	97	3
Patient 2	44	41	101	72	0	75	25
Patient 3	33	36	72	54	3	97	0
Type 2 fibers							
Patient 1	66	22	79	56	3	85	12
Patient 2	56	49	117	84	0	43	57
Patient 3	128	10	138	68	10	63	27

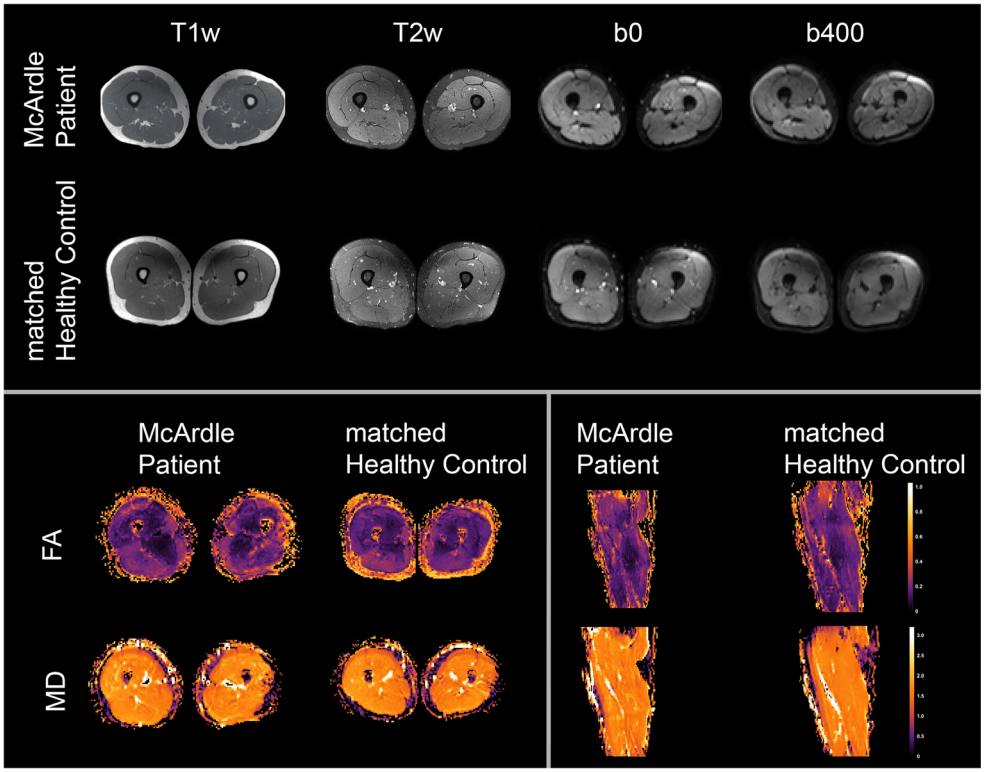

Fig. 3 Top row: T1w, T2w, and DW images of a McArdle patient and a healthy control. Bottom row: processed MD and FA heat maps in axial and sagittal views

10^{-3} mm^2/s (mean 1.569 ± 0.114), and RD ranged from 0.713 to 1.663 10^{-3} mm^2/s (mean 1.378 ± 0.128) for all muscles.

When post hoc two-sample Student's *t* tests for all parameters and muscles were performed, no parameter showed a significant deviation of patients from controls ($p > 0.05$) except for the FA of the left semimembranosus ($p = 0.048$). In this analysis, we did not correct for multiple comparisons, to ensure not missing any interesting findings, and reported the *p* values derived from Student's *t* tests. Box plots of the analyzed parameters are shown in Fig. 4, for each of the assessed muscles separately, taking together the same muscles from the left and right sides.

Discussion

In the current study, we evaluated DTI to detect altered water diffusion in the thigh muscles of McArdle patients compared to matched controls. Although histological analysis of biopsies of three of the McArdle patients showed intracellular glycogen accumulations within skeletal muscle fibers, we did not find any significant differences in the diffusion parameters of the thigh muscles.

Dystrophic and inflammatory myopathies with muscle edema, muscle cell necrosis with altered myofiber architecture, progressive muscle extracellular fibrosis, and lipomatous depositions unify different aspects of myopathodological changes. mDTI has been shown to be able to quantitatively capture some aspects of these pathologies. Specifically, in inflammatory muscle diseases (polymyositis and dermatomyositis), mDTI could show significantly higher apparent diffusion coefficient (ADC) values but no changes in FA values in affected/edematous muscles compared with healthy controls. A higher water content in muscle edema could thus be quantitatively captured with ADC values [18]. Li et al. could show that FA and ADC correlate with fatty infiltration of thigh muscles in children with Duchenne disease, whereas ADC did show a positive and FA a negative correlation with the percentage of fatty infiltration. They propose that the replacement of healthy muscle fibers by fibrous and adipose tissue destroys the physiological barriers that restrict water movement in those muscle fibers. As a result of this muscle destruction, the degree of water diffusion directionality is reduced (reduced FA values) and the overall water diffusion is increased (elevated ADC) [35]. Interestingly, Ponratrana et al. did find a positive correlation of mean fat fraction (MFF) with FA values and a negative correlation with MFF and ADC [23].

Froeling et al. could demonstrate that endurance exercise leads to changes in diffusion properties of the hamstring muscles after long-distance running, which could not be measured with standard T2w imaging, postulating that DTI provides additional information about myocellular changes that are neglected in the standard muscle-imaging protocols [21].

Since the pathophysiology of McArdle disease is based on altered glycogen metabolism, our main hypothesis was that glycogen accumulation or altered muscle fiber composition

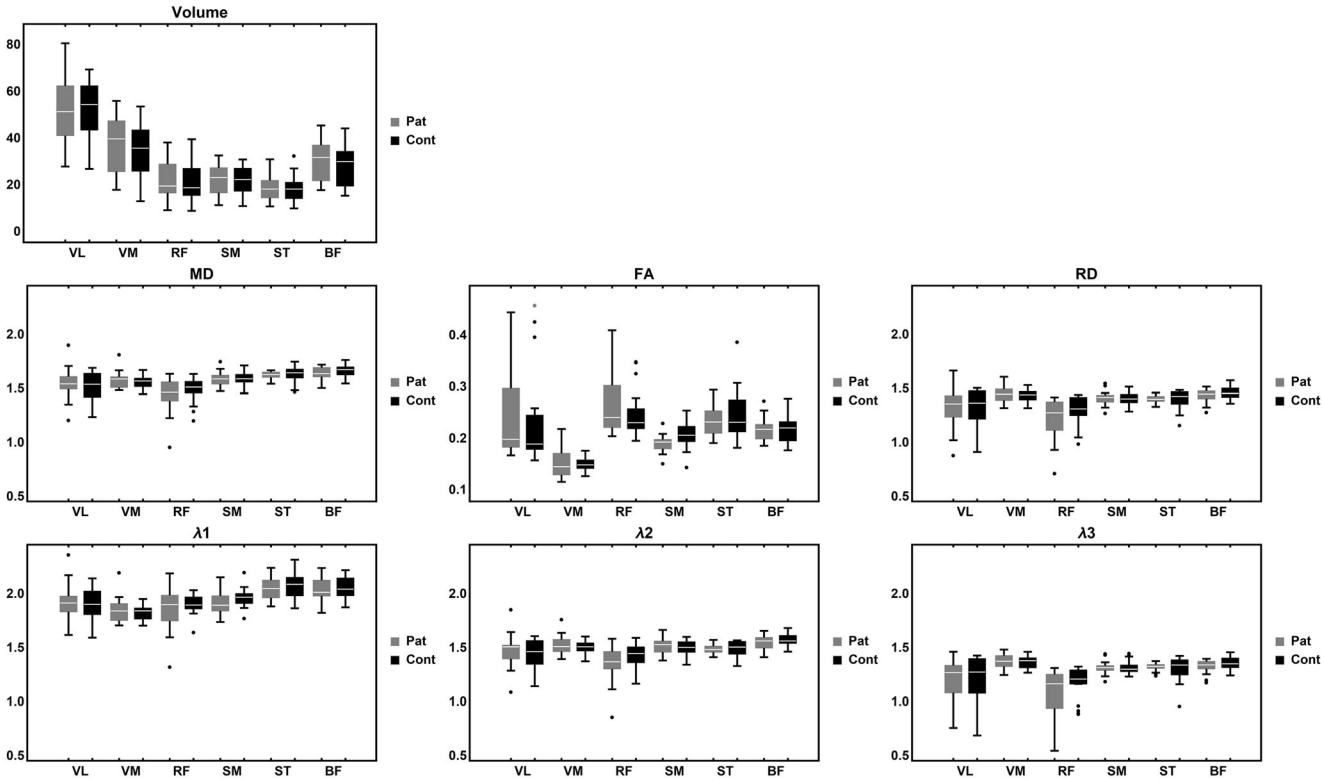

Fig. 4 Box plots of the assessed parameters for controls (gray) and McArdle patients (black). MD, mean diffusivity; FA, fractional anisotropy; RD, radial diffusivity; λ_{1-3}, eigenvalues 1–3; VL, vastus lateralis muscle; VM, vastus medial muscle; RF, rectus femoris muscle; SM, semimembranosus muscle; ST, semitendinosus muscle; BF, biceps femoris muscle. MD and RD λ_{1-3} are reported in 10^{-3} mm^2/s. Outliers are defined as 1.5 × IQR far outliers (light gray) and 3× IQR (see FA)

leads to altered focal water diffusion and to changes in the FA values in the measured muscles. Given most McArdle patients have a constantly elevated CK value, an additional hypothesis was that elevated CK values reflect myocellular damage and that this could be measured through elevated MD values as a representation of elevated diffusion. However, we did not find these effects in our present study. Furthermore, we could not find a difference in muscle volume in McArdle patients compared to controls.

Our biopsy data could show that especially type 2 fibers were prone to hypertrophy, whereas fiber atrophy was only present in up to 10% of both fiber types. DTI measurement of fiber type composition is especially sensitive for type 1 fibers, since they presuppose higher FA values due to a smaller diameter [36]. Berry et al. assessed the influence of muscle fiber diameter, edema, and fibrosis on the diffusion tensor variables (MD, FA, λ_{1-3}) in single- and multi-echo DTI sequence simulations [37]. They concluded that muscle fiber diameter inversely correlates with FA values up to a fiber diameter of 60 μm in simulations, which

Table 3 DTI data of patients and controls for lambda 1 (λ_1), lambda 2 (λ_2), lambda 3 (λ_3), mean diffusivity (MD), fractional anisotropy (FA), and SNR; each value is presented with a paired *t* test between patient and control groups

	Patient Mean ± SD	Control Mean ± SD	*p* values
SNR	38.668 ± 9.776	39.585 ± 8.667	0.398
λ_1	1.938 ± 0.154	1.950 ± 0.139	0.372
λ_2	1.481 ± 0.124	1.485 ± 0.099	0.766
λ_3	1.270 ± 0.150	1.284 ± 0.143	0.310
MD	1.566 ± 0.119	1.572 ± 0.108	0.594
FA	0.216 ± 0.060	0.215 ± 0.058	0.810

Table 4 Result table from ANCOVA: the mean square is an estimate of population variance. The *F* value represents the ratio of the variation between the sample means and the variation within the samples. R^2 indicates the percentage of how much variance can be explained by the tested parameter. The *p* values indicate the probability and would be significant when < 0.05

Between-subject effects

Variable	Mean squares	*F*	*p* value	R^2
λ_1	0.011	0.873	0.351	0.00368
λ_2	0.002	0.152	0.697	0.00064
λ_3	0.018	1.052	0.306	0.00444
MD	0.009	0.976	0.324	0.00412
FA	9.471E−05	0.034	0.855	0.00014
SNR	0.325	0.003	0.959	0.00001

could support our data where no significant effect on FA or the eigenvalues was seen despite histologically measured preponderance of type 2 fiber hypertrophy and no muscle fiber atrophy.

The voxel size in the DW images was $3 \times 3 \times 6$ mm^3 and thus did not allow capturing very localized intracellular diffusion changes. The constantly elevated CK values in McArdle patients suggest some damage to the muscle sarcolemma, but intramuscular glycogen accumulation and metabolic block of the intramuscular glycogen breakdown usually does not lead to a major disruption in muscle fiber integrity and progressive muscle fibrosis.

However, glycogen-affected muscle fibers are neighbored by healthy muscle fibers, which was also seen in our needle biopsy analysis [14]. Due to partial volume effects, these fibers with different stages of glycogen accumulation are captured within one voxel and the glycogen-loaded muscle fibers could be "overruled" by neighboring normal diffusion. Furthermore, our muscle biopsy showed that the glycogen deposits were intracellularly localized underneath the sarcolemma in a thin and crescent fashion and that there was no disruption of the sarcolemma and/or muscle fibrosis. Normal water diffusion could still be present in the center of the affected muscle fiber or between muscle fiber bundles and is not as impaired as in structural or inflammatory myopathies [18]. A combined MRI sequence measuring the diverse pathophysiology of muscle disease ranging from tissue inflammation over fibrosis to defects in metabolism has yet to be defined and would be beneficial for future studies [13, 38].

Limitations

Our study might be limited by the small sample size, since McArdle disease is a very rare muscle disease and our exclusion criteria were strict (no other disease, no diabetes). We did, however, recruit age- and gender-matched controls. De Kerviler et al. reported a higher degree of fatty infiltration in McArdle patients around the age of 50 in T1 imaging protocols [11]. A higher degree of fatty infiltration can affect FA values due to a reduced signal-to-noise ratio in fatty muscles. We therefore chose to evaluate patients at a younger age or without visible fatty infiltration of the leg muscles. Furthermore, we have used two fat suppression methods (SPAIR and gradient reversal). More recent articles suggest using triple fat suppression and/or acquiring Dixon data for fat quantification, which is of special benefit in the regions with residual artifacts (e.g., vastus lateralis and rectus femoris).

Conclusion

Despite intracellular glycogen accumulation in three assessed biopsy samples of patients, mDTI parameters were not altered in McArdle patients compared to controls. Therefore, we conclude that the currently used mDTI acquisition and processing lacks the sensitivity to detect intracellular changes due to accumulated glycogen in this cohort of McArdle patients. Due to the large diversity of muscular myopathies, there is still a need to validate different quantitative imaging sequences for different muscle diseases to investigate which methods allow detection of subtle muscle changes.

Acknowledgments We thank Philips Germany, especially Burkhard Maedler, for continuous scientific support.

Funding This study has received funding from FoRUM (research grant by Ruhr-University Bochum), Grant Number: F867R-2016.

Compliance with ethical standards

Guarantor The scientific guarantor of this publication is Prof. Matthias Vorgerd.

Conflict of interest The authors declare that they have no competing interests.

Statistics and biometry No complex statistical methods were necessary for this paper.

Informed consent Written informed consent was obtained from all subjects (patients) in this study.

Ethical approval Institutional review board approval was obtained.

Methodology
- Prospective
- Cross-sectional study
- Performed at one institution

References

1. De Castro M, Johnston J, Biesecker L (2015) Determining the prevalence of McArdle disease from gene frequency by analysis of next generation sequencing data: McArdle prevalence by NGS data. Genet Med 17:1002–1006
2. Quinlivan R, Buckley J, James M et al (2010) McArdle disease: a clinical review. J Neurol Neurosurg Psychiatry 81:1182–1188
3. Lebo RV, Gorin F, Fletterick RJ et al (1984) High-resolution chromosome sorting and DNA spot-blot analysis assign McArdle's syndrome to chromosome 11. Science (80-) 225:57–59
4. McArdle B (1951) Myopathy due to a defect in muscle glycogen breakdown. Clin Sci 10:13–35
5. Preisler N, Haller RG, Vissing J (2015) Exercise in muscle glycogen storage diseases. J Inherit Metab Dis 38:551–563
6. Godfrey R, Quinlivan R (2016) Skeletal muscle disorders of glycogenolysis and glycolysis. Nat Rev Neurol 12:393–402
7. Leite A, Oliveira N, Rocha M (2012) McArdle disease: a case report and review. Int Med Case Rep J 5:1–4
8. Nogales-Gadea G, Santalla A, Ballester-Lopez A et al (2016) Exercise and preexercise nutrition as treatment for McArdle disease. Med Sci Sports Exerc 48:673–679

9. Quinlivan R, Martinuzzi A, Schoser B (2014) Pharmacological and nutritional treatment for McArdle disease (Glycogen Storage Disease type V). Cochrane Database Syst Rev 12:CD003458
10. Vorgerd M, Zange J (2007) Treatment of glycogenosys type V (McArdle disease) with creatine and ketogenic diet with clinical scores and with 31P-MRS on working leg muscle. Acta Myol 26: 61–63
11. De Kerviler E, Leroy-Willig A, Duboc D, Eymard B, Syrota A (1996) MR quantification of muscle fatty replacement in McArdle's disease. Magn Reson Imaging 14:1137–1141
12. Nadaj-Pakleza AA, Vincitorio CM, Laforêt P et al (2009) Permanent muscle weakness in McArdle disease. Muscle Nerve 40:350–357
13. Zange J, Grehl T, Disselhorst-Klug C et al (2003) Breakdown of adenine nucleotide pool in fatiguing skeletal muscle in McArdle's disease: a noninvasive 31P-MRS and EMG study. Muscle Nerve 27:728–736
14. Heinicke K, Dimitrov IE, Romain N et al (2014) Reproducibility and absolute quantification of muscle glycogen in patients with glycogen storage disease by 13C NMR spectroscopy at 7 tesla. PLoS One 9:e108706
15. Lewis SF, Haller RG, Cook JD, Nunnally RL (1985) Muscle fatigue in McArdle's disease studied by 31P-NMR: effect of glucose infusion. J Appl Physiol (1985) 59:1991–1994
16. Gruetter R, Kaelin P, Boesch C, Martin E, Werner B (1990) Noninvasive31P magnetic resonance spectroscopy revealed McArdle disease in an asymptomatic child. Eur J Pediatr 149:483–486
17. de Kerviler E, Leroy-Willig A, Jehenson P, Duboc D, Eymard B, Syrota A (1991) Exercise-induced muscle modifications: study of healthy subjects and patients with metabolic myopathies with MR imaging and P-31 spectroscopy. Radiology 181:259–264
18. Ai T, Yu K, Gao L et al (2014) Diffusion tensor imaging in evaluation of thigh muscles in patients with polymyositis and dermatomyositis. Br J Radiol 87:20140261
19. Budzik JF, Balbi V, Verclytte S, Pansini V, Le Thuc V, Cotten A (2014) Diffusion tensor imaging in musculoskeletal disorders. Radiographics 34:E56–E72
20. Damon BM, Froeling M, Buck AKW et al (2016) Skeletal muscle diffusion tensor-MRI fiber tracking: rationale, data acquisition and analysis methods, applications and future directions. NMR Biomed 30:1–13
21. Froeling M, Oudeman J, Strijkers GJ et al (2015) Muscle changes detected with diffusion-tensor imaging after long-distance running. Radiology 274:548–562
22. Hooijmans MT, Damon BM, Froeling M et al (2015) Evaluation of skeletal muscle DTI in patients with Duchenne muscular dystrophy. NMR Biomed:1589–1597. https://doi.org/10.1002/nbm.3427
23. Ponrartana S, Ramos-Platt L, Wren TA et al (2015) Effectiveness of diffusion tensor imaging in assessing disease severity in Duchenne muscular dystrophy: preliminary study. Pediatr Radiol 45:582–589
24. Bergström J (1975) Percutaneous needle biopsy of skeletal muscle in physiological and clinical research. Scand J Clin Lab Invest 35: 609–616
25. Ekblom B (2017) The muscle biopsy technique. Historical and methodological considerations. Scand J Med Sci Sports 27:458–461
26. Shanely RA, Zwetsloot KA, Triplett NT, Meaney MP, Farris GE, Nieman DC (2014) Human skeletal muscle biopsy procedures using the modified Bergström technique. J Vis Exp 10:51812
27. Schlaffke L, Rehmann R, Froeling M et al (2017) Diffusion tensor imaging of the human calf: variation of inter- and intramuscle-specific diffusion parameters. J Magn Reson Imaging 4:1137–1148 https://doi.org/10.1002/jmri.25650
28. Damon BM (2008) Effects of image noise in muscle diffusion tensor (DT)-MRI assessed using numerical simulations. Magn Reson Med 60:934–944
29. Froeling M, Nederveen AJ, Nicolay K, Strijkers GJ (2013) DTI of human skeletal muscle: the effects of diffusion encoding parameters, signal-to-noise ratio and T2 on tensor indices and fiber tracts. NMR Biomed 26:1339–1352
30. Froeling M, Nederveen AJ, Heijtel DF et al (2012) Diffusion-tensor MRI reveals the complex muscle architecture of the human forearm. J Magn Reson Imaging 36:237–248
31. Veraart J, Novikov DS, Christiaens D, Ades-Aron B, Sijbers J, Fieremans E (2016) Denoising of diffusion MRI using random matrix theory. Neuroimage 142:394–406
32. Leemans A, Jones DK (2009) The B-matrix must be rotated when correcting for subject motion in DTI data. Magn Reson Med 61: 1336–1349
33. Veraart J, Sijbers J, Sunaert S, Leemans A, Jeurissen B (2013) Weighted linear least squares estimation of diffusion MRI parameters: strengths, limitations, and pitfalls. Neuroimage 81:335–346
34. Froeling M, Tax CMW, Vos SB, Luijten PR, Leemans A (2017) "MASSIVE" brain dataset: multiple acquisitions for standardization of structural imaging validation and evaluation. Magn Reson Med 77:1797–1809
35. Li GD, Liang YY, Xu P, Ling J, Chen YM (2016) Diffusion-tensor imaging of thigh muscles in Duchenne muscular dystrophy: correlation of apparent diffusion coefficient and fractional anisotropy values with fatty infiltration. AJR Am J Roentgenol 206:867–870
36. Scheel M, Winkler T, Scheel M et al (2013) Fiber type characterization in skeletal muscle by diffusion tensor imaging. NMR Biomed 26:1220–1224
37. Berry DB, Regner B, Galinsky V, Ward SR, Frank LR (2018) Relationships between tissue microstructure and the diffusion tensor in simulated skeletal muscle. Magn Reson Med 80:317–329
38. Jehenson P, Leroy-Willig A, de Kerviler E, Duboc D, Syrota A (1993) MR imaging as a potential diagnostic test for metabolic myopathies: importance of variations in the T2 of muscle with exercise. Am J Roentgenol 161:347–351